

# Engineered scaffolds based on mesenchymal stem cells/preosteoclasts extracellular matrix promote bone regeneration

Journal of Tissue Engineering  
Volume 11: 1–13  
© The Author(s) 2020  
Article reuse guidelines:  
sagepub.com/journals-permissions  
DOI: 10.1177/2041731420926918  
journals.sagepub.com/home/tej



Rui Dong<sup>1\*</sup>, Yun Bai<sup>1\*</sup>, Jingjin Dai<sup>1</sup>, Moyuan Deng<sup>2</sup>, Chunrong Zhao<sup>1</sup>, Zhansong Tian<sup>1</sup>, Fanchun Zeng<sup>1</sup>, Wanyuan Liang<sup>1</sup>, Lanyi Liu<sup>1</sup> and Shiwu Dong<sup>1,2,3</sup> 

## Abstract

Recently, extracellular matrix-based tissue-engineered bone is a promising approach to repairing bone defects, and the seed cells are mostly mesenchymal stem cells. However, bone remodelling is a complex biological process, in which osteoclasts perform bone resorption and osteoblasts dominate bone formation. The interaction and coupling of these two kinds of cells is the key to bone repair. Therefore, the extracellular matrix secreted by the mesenchymal stem cells alone cannot mimic a complex bone regeneration microenvironment, and the addition of extracellular matrix by preosteoclasts may contribute as an effective strategy for bone regeneration. Here, we established the mesenchymal stem cell/preosteoclast extracellular matrix -based tissue-engineered bones and demonstrated that engineered-scaffolds based on mesenchymal stem cell/preosteoclast extracellular matrix significantly enhanced osteogenesis in a 3 mm rat femur defect model compared with mesenchymal stem cell alone. The bioactive proteins released from the mesenchymal stem cell/preosteoclast extracellular matrix based tissue-engineered bones also promoted the migration, adhesion, and osteogenic differentiation of mesenchymal stem cells in vitro. As for the mechanisms, the iTRAQ-labeled mass spectrometry was performed, and 608 differentially expressed proteins were found, including the IGFBP5 and CXCL12. Through in vitro studies, we proved that CXCL12 and IGFBP5 proteins, mainly released from the preosteoclasts, contributed to mesenchymal stem cells migration and osteogenic differentiation, respectively. Overall, our research, for the first time, introduce pre-osteoclast into the tissue engineering of bone and optimize the strategy of constructing extracellular matrix-based tissue-engineered bone using different cells to simulate the natural bone regeneration environment, which provides new sight for bone tissue engineering.

## Keywords

MSC/POC ECM-based TEB, bone regeneration, extracellular matrix proteins, IGFBP5, CXCL12

Date received: 2 January 2020; accepted: 26 April 2020

## Introduction

The effective repair of bone defects is a challenge in orthopaedic surgery.<sup>1,2</sup> In recent years, several drawbacks have been observed in traditional tissue engineering techniques based on living mesenchymal stem cells (MSCs) such as insufficient oxygen and blood flow in the microenvironment within the defected bone. These contribute to the death of a high percentage of MSCs, ultimately leading to the failure of treatment. Moreover, a limitation also exists in storage and transportation due to the viability of MSCs.<sup>3</sup>

In order to solve the above issues, our group used lyophilization to develop extracellular matrix (ECM)-based

<sup>1</sup>Department of Biomedical Materials Science, School of Biomedical Engineering, Third Military Medical University, Chongqing, China

<sup>2</sup>Department of Orthopedics, Southwest Hospital, Third Military Medical University, Chongqing, China

<sup>3</sup>State Key Laboratory of Trauma, Burns and Combined Injury, Third Military Medical University, Chongqing, China

\*These authors contributed equally to this work

### Corresponding author:

Shiwu Dong, Department of Biomedical Materials Science, School of Biomedical Engineering, Third Military Medical University, Gaotanyan Street No. 30, Chongqing 400038, China.

Email: dongshiwu@tmmu.edu.cn



tissue engineered bone (TEB). There are a variety of methods to obtain ECM. Relative to chemical/enzymatic treatment, freeze-thaw cycles, and mechanical disruption, lyophilization is a moderate physical treatment for preserving most proteins. The destruction of cells and DNA reduces the antigenicity, but most active proteins remain.<sup>4,5</sup> ECM works as a reservoir of growth factors and cytokines, which send signals that regulate cell proliferation and migration as well as cell differentiation.<sup>6</sup> Bone repair is a dynamic process involving multiple cells. The survival, homing, and differentiation of MSCs are critical in the success of tissue engineering.<sup>7</sup> However, the ECM secreted by the MSCs alone cannot mimic a complex bone regeneration microenvironment. Recent studies have shown that the coupling of osteoblasts and osteoclasts plays a crucial role in bone remodelling and bone repair.<sup>8</sup>

Osteoclasts (OCs) were initially thought to be harmful to bone regeneration. With the deciphering of mechanisms that control osteoclast differentiation, we have found that the role of OCs in bone regeneration is indispensable. Recent studies demonstrated that OCs might directly regulate osteoblast differentiation, the hematopoietic stem cell (HSC) niche, T-cell activation, and the proliferation of tumour and stromal cells in bone.<sup>9–12</sup> Interestingly, it was observed that the cortical bones of *Csf1*<sup>-/-</sup> mice were fragile, in which the OCs were found to be depleted. Platelet-derived growth factor-BB (PDGF-BB) from tartrate-resistant acid phosphatase (TRAP<sup>+</sup>) preosteoclasts residing on the bone surface is capable of temporally and spatially coordinating osteogenesis accompanied by angiogenesis during bone growth, modelling, and remodelling.<sup>13</sup> The depletion of mature OCs but the restoration of POCs is on the uptrend in treating osteoporosis.<sup>14</sup>

In the present study, we cocultured POCs and MSCs to establish MSC/POC ECM-based TEB. This study aims to investigate the effect of MSC/POC on the ECM protein profile in order to explore a better cell combination for optimizing the engineered ECM-based scaffolds.

## Materials and methods

### Animals and cells

Four-week-old C57BL/6 mice and 2-month-old Sprague Dawley (SD) rats were purchased from Animal Center of the Third Military Medical University (Specific Pathogen Free laboratory). The laboratory animal use license number is SYXK (Chongqing) 20170002. The animal laboratory adopts the new wind central air conditioning ventilation system, and the temperature is 20–26°C, and the relative humidity is 40%–70%. All the animals were free to move, eat, and drink and treated with the guidelines of Third Military Medical University laboratory animal care and use. Mouse bone marrow-derived MSCs (BMMSCs) were isolated from the tibia and femur of C57BL/6 mice by flushing with Dulbecco's Modified

Eagle Medium (DMEM, HyClone, Logan City, Utah, USA) supplemented with 10% fetal bovine serum (FBS, Thermo Fisher Scientific, Waltham, Massachusetts, USA), 100 U/mL penicillin (Millipore-Sigma, Burlington, MA, USA), and 100 g/mL streptomycin sulfate (Millipore-Sigma), after removal of the epiphysis at both ends. All suspension cells from bone marrow were seeded into 25 cm<sup>2</sup> cell culture flasks and cultured in a humidified incubator (5% CO<sub>2</sub> at 37°C). After 3 days, the floating cells were removed, and the adherent cells were cultured for 1 week, with the fresh medium replaced every other day. When BMMSCs reached 80% density, cells were passaged for further expansion.

Bone marrow monocytes (BMMNCs) were separated by flushing bone marrow cells from 4-week-old C57BL/6 mouse femurs and tibia. The BMMNCs were cultured with  $\alpha$ -MEM supplemented with 10% FBS and maintained in a humidified incubator at 37°C in 5% CO<sub>2</sub> for 6 h. The adherent cells were removed, and non-adherent cells were cultured with macrophage colony-stimulating factor (M-CSF, 30 ng/mL) and receptor activator of nuclear factor kappa-B ligand (RANKL, 100 ng/mL) for 48 h to obtain preosteoclasts (TRAP<sup>+</sup> mononuclear cells) for subsequent experiments according to Jie Huang et al.<sup>15</sup>

### Preparation of ECM-based TEBs

Decalcified bone matrix (DBM, Aojing Pharmaceutical Technology, Beijing, China) was used as the scaffold material. To obtain ECM-based TEBs with varying maturity, MSCs and MSCs plus the POCs complex at a ratio of 10:1 were seeded onto the scaffolds at 10<sup>6</sup> cells per scaffold and were further cultured with osteogenic differentiation medium for C57BL/6 mouse BMMSCs (Cyagen Biosciences, China) for 7 or 14 days, respectively, that is,  $\alpha$ -MEM medium supplemented with 10% fetal bovine serum, 1% penicillin-streptomycin, 0.05 mM ascorbate, 10 mM  $\beta$ -Glycerophosphate and 100 nM dexamethasone. Then, the cell-based scaffolds on 1 week or 2 weeks were lyophilized to generate 7d ECM-based TEBs and 14d ECM-based TEBs. The process of lyophilization included rinsing of cell-based scaffolds in phosphate buffered saline (PBS), freezing at -80°C, lyophilizing for 24 h under sterile conditions followed by storage at -80°C for 3 months to reduce immunogenicity.<sup>16</sup>

### Surface morphology of ECM-based TEB

ECM-based TEBs and DBMs were fixed with glutaraldehyde, dehydrated in a gradient, and sealed with tert-butyl alcohol. The scaffolds were then sprayed with gold and examined using a scanning electron microscope (S3400 N II; Hitachi, Tokugawa, Japan) with an accelerating voltage of 15 kV and a working distance of 20–30 mm.

### Mixed lymphocyte reaction (MLR) assay

The design of MLR assay was according to Thaweesapphithak et al.<sup>17</sup> BALB/c spleen lymphocytes (SLCs) were treated with mitomycin C (50 µg/mL, Sigma) for 30 min at 37°C as stimulator cells. C57BL/6 SLCs were incubated with 0.5 µM 5(6)-carboxyfluorescein diacetate *N*-succinimidyl ester (CFSE, Sigma, St. Louis, MO) at 37°C for 15 min as responder cells. Stimulator and responder cells were co-cultured at a ratio of 1:1 in 96-well plates ( $5 \times 10^5$  cells/well). The mixed lymphocytes were incubated with RPMI 1640 medium and distributed to the following 6 groups: (1) vehicle control group (mixed DBMs with SLCs), (2) PHA (phytohemagglutinin, mixed SLCs incubated with 10 µg/mL PHA), (3) MSC-based TEBs (mixed SLCs with MSC-based TEBs), (4) MSC/POC-based TEBs (mixed SLCs with MSC/POC-based TEBs), (5) MSC ECM-based TEBs (mixed SLCs with MSC ECM-based TEBs), and (6) MSC/POC ECM-based TEBs (mixed SLCs with MSC/POC ECM-based TEBs). The cells were incubated with RPMI 1640 medium for five days, and cell viability was determined using a cell counting kit-8 (CCK-8) assay kit (Jiancheng Biotechnology, Nanjing, China).

### Fluorescence of MHC-I, MHC-II and DNA

ECM-based TEBs were fixed with 4% paraformaldehyde and then incubated with PBS containing 0.3% Triton X-100 (Millipore Sigma) and 10% mouse serum albumin to allow cells to transmit and block interactions with nonspecific proteins. Next, scaffolds were incubated with specific antibodies against major histocompatibility complex-I and II (MHC-I and MHC-II, Biosciences, Heidelberg, Germany) and then incubated with secondary antibody and 4,6-diamidino-2-phenylindole (DAPI, Sigma) in the dark. Finally, MHC-I, MHC-II protein, and DNA were detected with a fluorescence microscope.

### DNA quantification assay

Measuring the amount of double-stranded DNA (dsDNA) in the decellularized-extracellular matrix (dECM) is the current gold standard for evaluating the degree of successful decellularization. Samples were divided into five groups: DBMs, 14d MSC-based TEBs, 14d MSC ECM-based TEBs, 14d MSC/POC-based TEBs, 14d MSC/POC ECM-based TEBs. Samples (~10 mg) were transferred to 1.5 mL Eppendorf tube and digested in 250 mg/mL papain (Sigma-Aldrich) overnight at 60°C. Quant-iT<sup>TM</sup> PicoGreen<sup>®</sup> dsDNA Reagent and Kits (Invitrogen, Carlsbad, California, USA) was employed according to the manufacturer's protocol, and the fluorescence was quantified at 520 nm with excitation at 480 nm.

### In vivo examination

Rats were randomly divided into three groups ( $n=6$ ): DBM without ECM proteins (blank control, cultured in the osteogenic induction medium for 14 d), MSC ECM-based TEB, and MSC/POC ECM-based TEB were implanted into the defects and further survived for 3 weeks and 8 weeks. To study the regeneration of in situ femoral defects, SD rats were anaesthetized intraperitoneally with 0.5% sodium pentobarbital at a dose of 15 mg/kg and disinfected with iodophor. The rats were fixed on the operating table, and both limbs were flexed their knees 90 degrees. Made a 1 cm long incision on both sides of the knee joint to cut the skin, subcutaneous tissue, and bluntly separated the muscle and sarcolemma to fully expose the lower end of the femur, including the femoral condyle. The position of the femur was tightly fixed with tweezers, and a cylindrical penetrating defect with a diameter of 3 mm was made from the outside of the femoral condyle with a dental drill. In the repair experiment, we put the two ECM-based TEBs or two DBMs (3 mm×3 mm×3 mm porous scaffold) into the defect (the volume of the defect was about 60 mm<sup>3</sup>, the volume of two scaffolds was about 54 mm<sup>3</sup>). After the operation, the myometrium and skin were rinsed with normal saline and the skin was sutured. After the rats were awakened, they were kept in cages under the same conditions. Finally, rats were sacrificed, femurs from each group were collected and fixed with 4% paraformaldehyde for micro-computed tomography (micro-CT) analysis. After micro-CT, samples were decalcified with 10% w/v acid (ethylenediaminetetraacetic acid (EDTA)) solution, using a series of increasing concentrations of ethanol solution (50%–100%). The xylene was dehydrated and finally embedded in paraffin for histological examination. Sections were obtained from paraffin blocks using a microtome (Leica RM2125 RTS, Germany) and stained with Masson's three colours (MT) to investigate the repair of bone defects. Fixed specimens were scanned in a micro-CT (GE phoenix v—tome—x, Germany) using X-ray radiation (source voltage 85 kV and beam current 75 µA) to obtain 3D imaging to assess the quality of new bone formation. Quantitative assessment of osseointegration at the defective region of interest (ROI) had a scan resolution of 25 µm. Bone volume fraction, trabecular thickness, trabecular bone number, and trabecular bone separation were calculated using VGStudio MAX (Volume Graphics, Germany) software.

### Preparation of ECM-based TEB extract and quantitation of total proteins

7d MSC ECM-based TEBs, 7d MSC/POC ECM-based TEBs, 14 d MSC ECM-based TEBs and 14d MSC/POC ECM-based TEBs were initially immersed in 2 mL PBS and broken up into turbid liquid with an ultrasonic oscillator. Then samples ( $n=20$ ) were centrifuged at 4°C with

13,000 rpm for 30 min and reserved the supernatant. The total protein concentration of the supernatant was then determined using a bicinchoninic acid (BCA) protein assay kit (CW BIO, Beijing, China). To eliminate the effect of different supernatant protein concentrations on cell behaviors, we normalized the supernatant protein concentration to 1 mg/mL with PBS for subsequent experiments.

### Cell proliferation assay

The extract of ECM-TEBs was placed separately on the upper chamber of a 24-well transwell plate (0.4  $\mu$ m, Millipore). BMMSCs were seeded at the bottom of the wells at  $10^5$  cells/well and cultured in osteogenic differentiation induction medium. Cell proliferation was determined by the CCK-8 assay kit on days 1, 3, 5, and 7.

### Transwell assay

Cell migration was estimated in the 24-well transwell plates (8 microns, Millipore, Darmstadt, Germany). BMMSCs were resuspended in serum-free medium at  $10^4$  cells/mL and 1 mL of cell suspension was placed in the upper chamber. The extract of the DBMs or ECM-based TEBs was placed in the lower chamber. Twenty-four hours later, cells migrating to the underside of the filter were fixed with 4% paraformaldehyde and stained with DAPI. The number of migrated cells was counted in five different fields under a microscope ( $\times 200$ ), and the data were averaged from three parallel experiments.

### Wound healing assay

ECs ( $10^6$  cells/well) were seeded on 6-well plates and incubated at 37°C. When the cells reached 90% density, the cell surface was scraped with a 200  $\mu$ L pipette tip and the cells were washed with PBS to remove debris. The extract of DBMs or ECM-based TEBs and the serum-free medium were mixed at a ratio of 1:1 to prepare a culture medium and 2 mL of this medium was added to each well. The changes in scratch were observed and recorded with a microscope at  $t=0$  and 12 h. ImageJ was used to measure the scratch area. Scratch healing ratio (%) =  $(A_0 - A_{12}) / A_0 \times 100\%$ , where  $A_0$  represents the initial scratch area ( $t=0$  h) and  $A_{12}$  represents the final scratch area at  $t=12$  h. Five non-overlapping fields were randomly taken from each dish, and the test was repeated for three times.

### Cell adhesion detection

To evaluate the cell adhesion capacity of ECM-based TEBs, we performed the oscillatory cell adhesion assay and prepared 10 composites for each group. MSCs ( $10^5$  cells/mL, 30  $\mu$ L) were seeded onto the two types of ECM-based TEB and then cultured for 5 min at 37°C. Five cell-scaffold composites in each group were randomly selected

to 50 mL centrifuge tubes, which were filled with 10 mL of the basic culture medium and shaken at 150 r/min for 2 min with the orbital shaker to remove the non-adherent cells. Then, all of the ECM-based TEBs, with or without the shaking, were removed and re-cultivated in a new 6-well plate. Finally, cells with ECM-based TEBs were further cultured for 4 h, and the number of cells was determined by the CCK-8 assay kit.

### Osteogenic differentiation of BMMSCs

The normalized extract of the 14d ECM-based TEBs was placed on the upper Boyden chamber of a 24-well plate (0.4  $\mu$ m, Millipore). MSCs ( $10^5$  cells/well) were cultured at the bottom of the wells and incubated with osteogenic differentiation induction medium. After 14 days, ALP staining and Alizarin Red S staining were performed to assess ALP activity and calcium deposition from MSCs, respectively. And total RNA extracted by RNAiso Plus Reagent (Takara, Kyoto, Japan). cDNA was synthesized from 1 mg of total RNA using a PrimeScript Real-Time Reagent Kit (Takara) according to the manufacturer's instructions. Real-time quantitative PCR was performed using SYBR Premix Ex Taq (Takara). The PCR amplifications were carried out by the mRNA-specific primers as follows: Runx2 (forward) 5'-AGGCAGGTGCTTCAGAA

CTGGG-3,' (reverse) 5'-GCTGGGTAGTGCATTCGTGGGT-3'; Osx (forward) 5'-CCCCACCCCTTAGACA

CCATGAC-3,' (reverse) 5'-TGCACCCCCAAACCAA

TGTCCTC-3'; Col1a1 (forward) 5'-GACCTGTGTGT

TCCCCACTCA-3,' (reverse) 5'-TGGATAGCGACATCG

GGCAG-3' and GAPDH (forward) 5'-AGGTCGGTGT

GAACGGATTG-3,' (reverse) 5'-TGTAGACCATGTA

GTTGAGGTCA-3.' GAPDH was used as a loading control.

### Protein expression profiling and bioinformatics analysis

The resultant peptide mixture of 14d MSC ECM-based TEBs and 14d MSC/POC ECM-based TEBs was labeled with an iTRAQ 6Plex labeling kit (Sciex, Beijing, China) and then subjected to high pH reverse phase separation and nano-HPLC-MS/MS analysis. Moreover, we repeated the experiments with three sets of biological replicates. The obtained data were subjected to hierarchical clustering of unsupervised proteins using the limma R package, then Gene Ontology (GO) analysis, and Kyoto Gene and Genome Encyclopedia (KEGG) pathway enrichment were performed using the cluster Profiler R package.

### In vitro release profiles of the cytokines IGFBP5 and CXCL12

14d MSC ECM-based TEBs and 14d MSC/POC ECM-based TEBs ( $n=10$ ) were individually placed into an

Eppendorf tube with 1 mL of PBS (pH 7.2) at 37°C and subjected to shaking at 50 rpm/min. We exchanged the 900 µL buffer with fresh medium on days 1, 2, 3, 5, 7, 9, 12, and 14. The cytokine concentrations were measured with enzyme-linked immunosorbent assay (ELISA) kits (ELH-IGFBP5-001, ELH-CXCL12-001; RayBiotech, Norcross, GA). The release profiles were generated based on the number of cytokines released or the cumulative release at individual incubation time points (RayBiotech).

### **Secretion of the cytokines IGFBP5 and CXCL12 assay**

BMMSCs and POCs were cocultured at a ratio of 10:1 in transwells with indirect contact and incubated with osteogenic induction medium for 14 days. The cells were refreshed with PBS, lysed with radioimmunoprecipitation assay (RIPA), and resuspended to obtain a protein solution. The variations in IGFBP5 and CXCL12 secreted by MSCs or POCs before and after coculture were detected by ELISA kits.

### **Biological function of IGFBP5 and CXCL12 assay**

For the IGFBP5 neutralizing assay, the control group was the extract of MSC/POC ECM-based TEB incubated with bovine serum albumin (BSA). The experimental group were MSC/POC ECM-based TEB extract pretreated with 10 µg/mL recombinant neutralizing mouse IGFBP-5 (R&D Systems, Minneapolis, USA) before the application of real-time PCR, Alizarin Red S staining and ALP staining.

For the CXCL12 neutralizing assay, the extract of MSC/POC ECM-based TEBs was treated with 10 µg/mL of the anti-mouse CXCL12/SDF-1 antibody (R&D Systems) or BSA, and the transwell assay and wound healing assay were performed.

### **Statistical analysis**

Unpaired two-tailed Student's t-test was used for comparison between two groups and one-way analysis of variance (ANOVA) with Bonferroni post hoc test was applied for multiple comparisons. Three independent experiments were used for the various in vitro experiments. The results were displayed as the mean ± standard deviation for n=3 samples per group in all cases unless otherwise indicated. For all the experiments,  $p < 0.05$  was considered to be significant and was indicated by '\*';  $p < 0.01$  was indicated by '\*\*'.

## **Results**

### **Fabrication and characterization of MSC/POC ECM-based TEBs**

In the present study, we first successfully induced BMMNCs into preosteoclasts, which were characterized

by TRAP-positive monocytes (Figure 1(a)) and then constructed MSC ECM-based TEBs and MSC/POC ECM-based TEBs.<sup>18</sup> The specific contents were as follows: BMMSCs were first implanted on DBMs and then the cell-based TEBs were decellularized. (Figure 1(b)).<sup>19</sup> POCs plus MSCs or MSCs alone were implanted on DBMs for up to 7 or 14 days and the result showed MSC/POC group accumulated abundant proteins at 14 days (Figure 1(c)). Typical cell coating was present on the surface of the scaffold under scanning electron microscopy, and only cell debris and extracellular matrix remained on the surface instead of normal cell morphology after decellularization (Figure 1(e)).

The results from MLR experiments suggested that lyophilization was effective in decreasing immunogenicity (Figure 1(d)). Almost no nuclear DNA was detected through DAPI staining in ECM-based TEBs. Besides, the fluorescence results suggested that the level of MHC-I and MHC-II antigens reduced significantly. The ECM-based TEBs showed lower antigenic components (MHC-I, MHC-II, and DNA fragments) and were more biocompatible than cell-based TEB (Figure 1(f)). Significantly decreased DNA content was observed after lyophilization and storing at -80°C for 3 months compared to those of the cell-based TEB. 14d MSC ECM-based TEBs and 14d MSC/POC ECM-based TEBs contained < 50 ng/mg dsDNA. Above all, we can conclude that samples have been sufficiently decellularized (Figure 1(g)).

### **In vivo bone regeneration capacity of MSC/POC ECM-based TEBs**

A rat bone defect model was established to investigate the therapeutic potential of MSC/POC ECM-based TEB in bone defects. The rats were sacrificed at 3 weeks and 8 weeks after implantation and their femurs were dissected. Newly formed bones were examined quantitatively by Micro-CT and evaluated qualitatively by Masson staining after decalcifying the femoral samples. Histological evidence showed that MSC/POC ECM-based TEBs increased the newly formed bone tissues, compared with the DBMs and MSC ECM-based TEBs (Figure 2(a) and (b)). Consistent with the Masson staining results, the 3D reconstructed view showed rarely new bones regenerated in the control group (Figure 2(c)), while moderate amounts of new bone appeared in the MSC group.

To our satisfaction, abundant new bone formation was observed within the femoral defect site, after implantation of the MSC/POC ECM-based TEBs. Quantitative analysis of BV/TV and the number of trabecular bones (Tb.N) showed a significant improvement in the MSC/POC group compared with the other groups. However, there were no apparent differences in trabecular thickness (Tb. Th) and trabecular separation (Tb. Sp) among the three groups (Figure 2(d)). All the above results indicated that MSC/

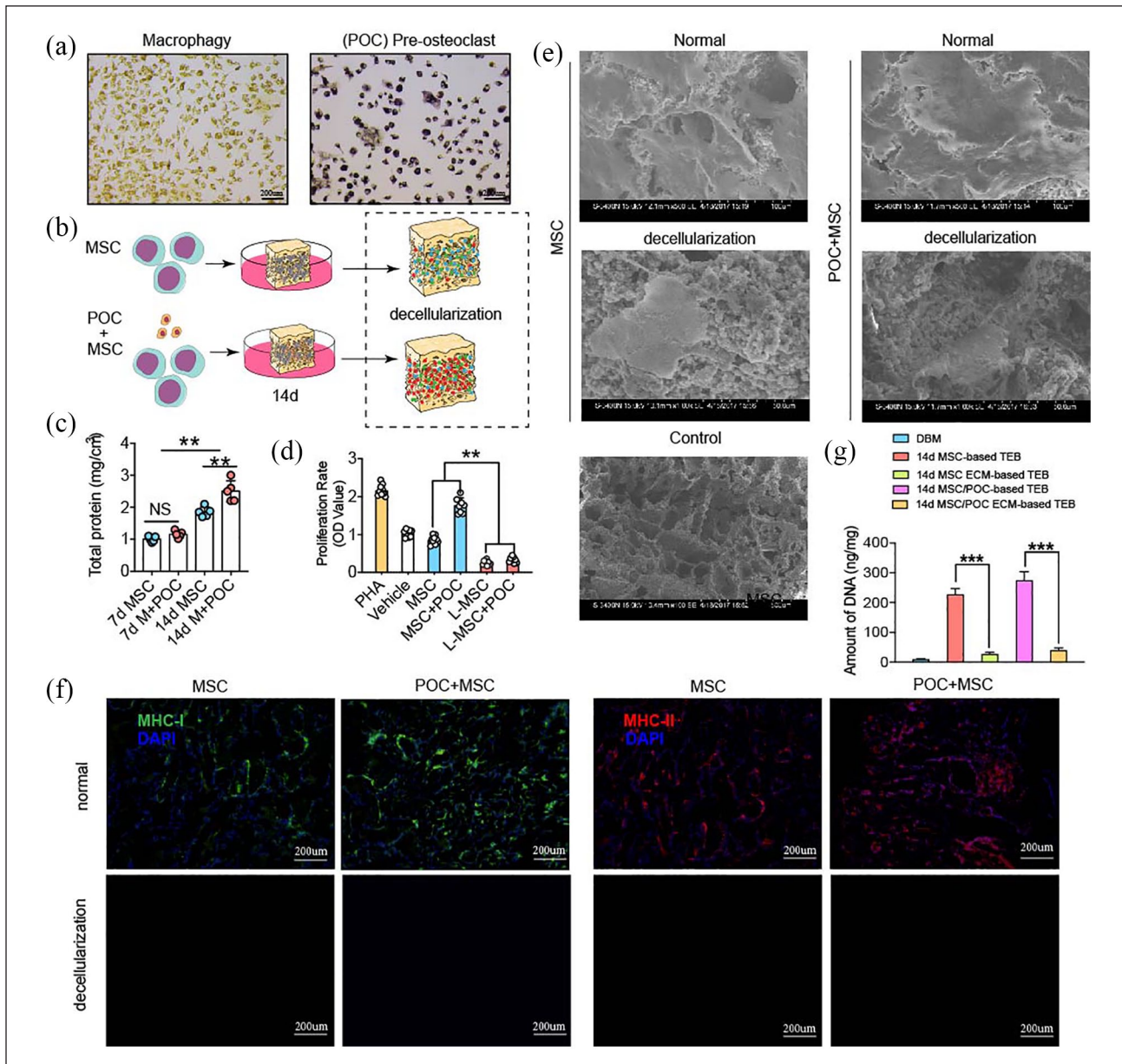


**Figure 1.** Fabrication and characterization of MSC/POC ECM-based TEBs. (a) Pre-osteoclasts (POCs) presented TRAP-positive staining. Scale bars: 200  $\mu$ m. (b) Schematic illustration of ECM-based TEB fabrication. (c) Quantitative analysis of the total proteins retained on ECM-based TEBs. (d) Biocompatibility analysis of ECM-based TEBs using a mixed lymphocyte reaction (MLR) assay. (e) Surface morphology of ECM-based TEBs under scanning electron microscopy (SEM). Scale bars are 100  $\mu$ m and 50  $\mu$ m. (f) Fluorescence staining of DAPI as well as MHC-I and MHC-II. Scale bars: 200  $\mu$ m. \*\* $p < 0.01$ , \* $p < 0.05$ , NS: no significance. (g) Quantification of DNA before and after lyophilization. DNA was nearly completely removed, \*\*\* $p < 0.001$ .

POC ECM-based TEBs significantly promoted bone regeneration *in vivo*.

#### Proteins released from MSC/POC ECM-based TEBs promoted the migration, adhesion and osteogenic differentiation of BMMSCs

In order to investigate the impact of maturity for seed cells on total protein deposition, we established two groups: cell-scaffold complex is cultured *in vitro* for 7 or 14 days.

The changes in the biological behavior of BMMSCs under the influence of deposited proteins were then explored. The proliferation assay results showed that the 14d MSC/POC group significantly enhanced the propagation of BMMSCs, and there was no discernible difference among 14d MSC group, 7d MSC group and 7d MSC/POC group (Figure 3(a)). BMMSCs recruited to the bone defect sites to participate in tissue repair and cell migration is critical for bone regeneration. Wound healing and transwell migration assay showed that MSC/POC ECM both at 7 days or

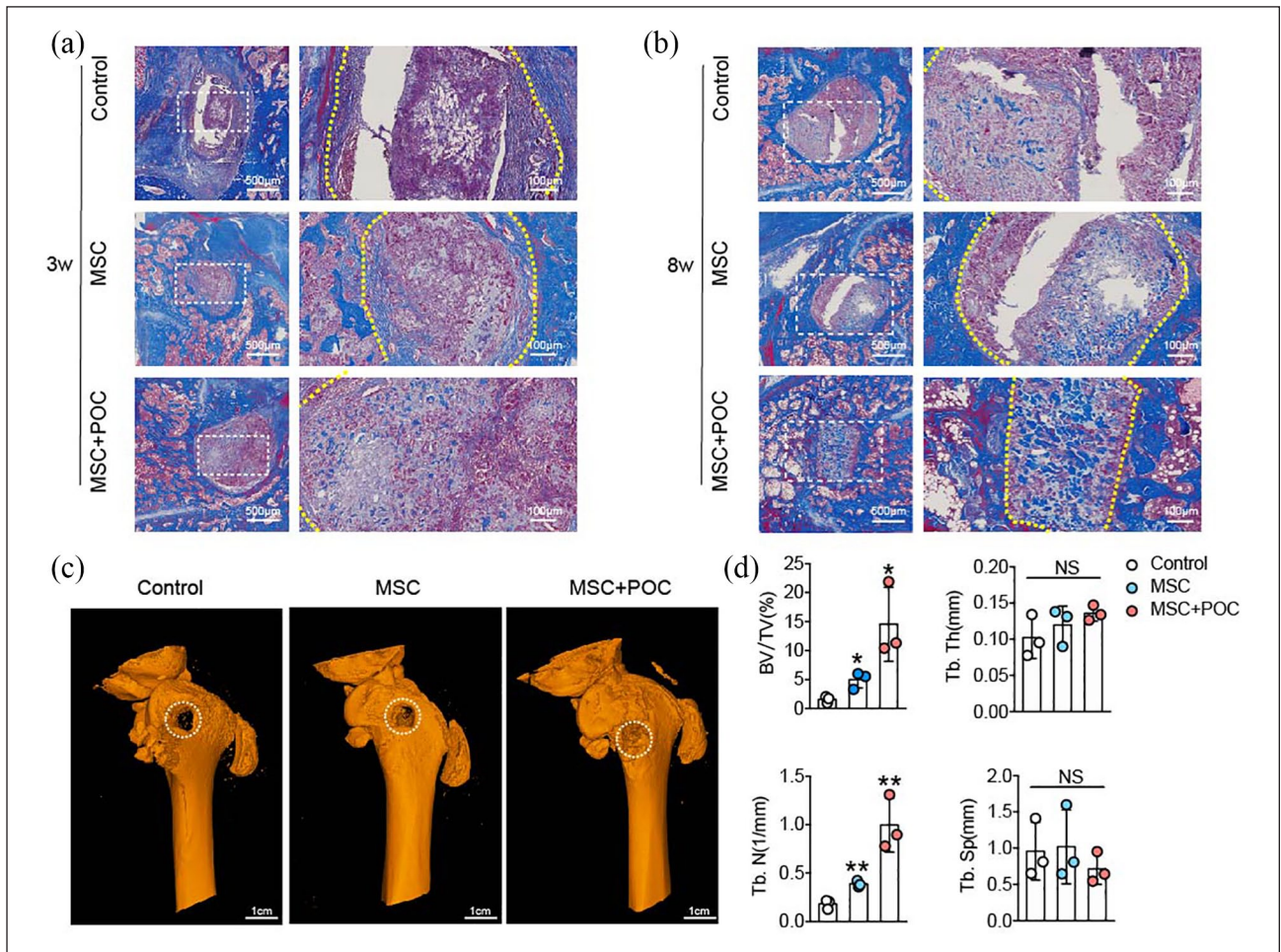


**Figure 2.** MSC/POC ECM-based TEBs promote bone regeneration *in vivo*. (a, b) Representative images of the Masson staining. Scale bars are 500  $\mu$ m and 100  $\mu$ m. (c) Representative images of 3D micro-CT reconstruction. Scale bars: 1 cm. (d) Quantitative analysis of micro-CT; \*\* $p < 0.01$ , \* $p < 0.05$ , NS: no significance.

14 days recruited more BMMSCs (Figure 3(b) and (c)). The analysis of the cell adhesion of two ECM-based TEBs revealed that the MSC/POC group conglomerated more BMMSCs on porous scaffolds (Figure 3(d)). As far as osteogenesis was concerned, marker genes Runx2, Col1a1, and Osx revealed that the MSC/POC group had advantages in osteogenic differentiation (Figure 3(e)) and ALP and Alizarin Red S staining results also verified this finding (Figure 3(f)). Thus, it can be concluded that the active proteins released from MSC/POC ECM-based TEBs enhanced proliferation, migration, adhesion, and osteogenic differentiation of BMMSCs.

### Proteomic analysis of ECM-based TEBs

Plenty of evidence has shown that MSC/POC ECM-based TEBs can repair bone defects more effectively than MSCs alone both *in vitro* and *in vivo*, yet it is unclear that which specific soluble active proteins of the extracellular matrix are responsible for such function. Hence, we performed an iTRAQ-labeled MS proteomic analysis to find out crucial

different components of ECM. First protein expressions were normalized and then differentially expressed proteins were compared between MSC/POC group and MSC group (Supplemental Table S1). An absolute value of  $\log_{2}FC \geq 0.1$  and a  $p$ -value  $< 0.05$  were set as a significantly different threshold. The volcano plot exhibited a differential protein profile (Figure 4(a)), in which the introduction of POCs caused dramatic changes in proteomics, with a total of 324 proteins upregulated and 284 proteins downregulated. Top 50 distinct proteins were listed in the form of a heat map (Figure 4(b)). Next, we conducted enrichment of functions and signalling pathways of the 608 differentially expressed proteins by Gene Ontology (GO). The Supplemental Table S2 listed the six major biological processes closely associated with osteogenesis included osteoblast differentiation, mesenchymal cell differentiation, mesenchymal development, tissue remodelling, and muscle cell proliferation and tissue of extracellular matrix, in which IGFBP5 accounted for a considerable proportion (Figure 4(c)). Besides, IGFBP5 has been reported to be closely related to osteoblast differentiation. Finally, an analysis of KEGG pathway

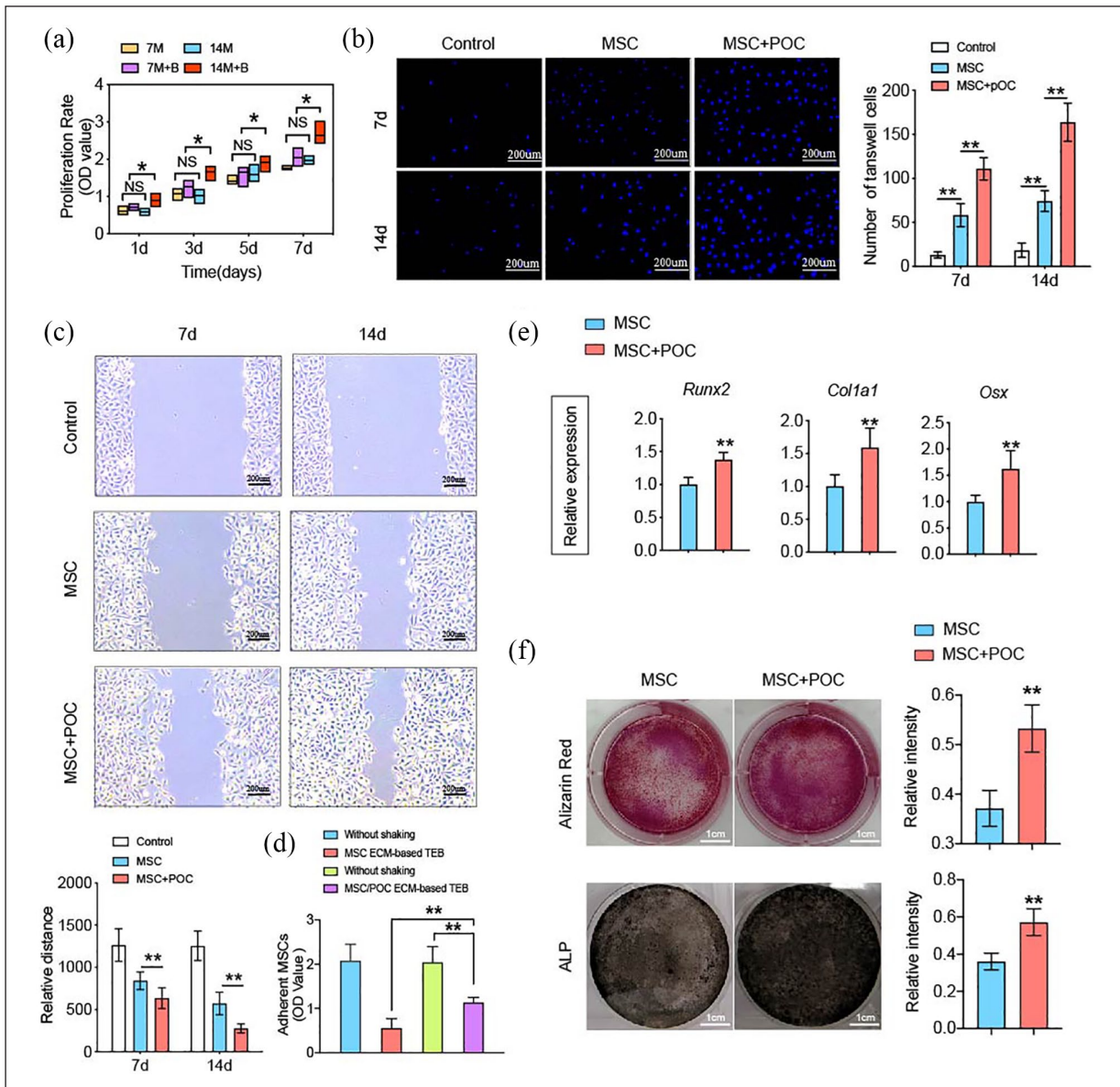


**Figure 3.** Proteins released from MSC/POC ECM-based TEBs promoted the migration, adhesion and osteogenic differentiation of MSCs. (a) Extracts from 14-d MSC/POC ECM-based TEBs enhanced the proliferation of MSCs as determined by the CCK-8 assay. (b) DAPI fluorescence of MSC invasion ability by the transwell assay. (c) Scratch area of ECs in different intervention groups at 0 h and 12 h after the scratch was made. Scale bars are 200 µm. (d) Adhesion capacity assessed by the proportion of cells retained in the scaffolds within 6 h. (e) Extracts from MSC/POC ECM-based TEBs enhanced osteogenic gene expression, including Runx2, Col1a1, and Osx, GAPDH was used as a loading control. (f) Representative images of MSCs osteogenic differentiation determined by Alizarin Red S staining and ALP staining. Scale bars are 1 cm. \*\* $p < 0.01$ , \* $p < 0.05$ , NS: no significance.

enrichment among the 608 differentially expressed proteins found that several pathways mainly reflected ‘cell adhesion’ and ‘cell migration’ such as rheumatoid arthritis, cell adhesion molecules (CAMs), ECM-receptor interactions, actin-regulated cytoskeleton, and leukocyte transendothelial migration (Supplemental Tables S3 and S4). Similarly, CXCL12 was identified as the most prominent player in KEGG pathway enrichment statistics, which closely related to cell migration (Figure 4(d)).

### *IGFBP5 and CXCL12 released from the MSC/POC ECM-based TEBs separately enhanced osteoblastic differentiation and migration of BMMSCs*

We first measured and mapped these two cytokines’ release profiles and cumulative total release from ECM-based TEB. The release of IGFBP5 from MSC/POC ECM-based TEBs sustained for approximately 12 days.

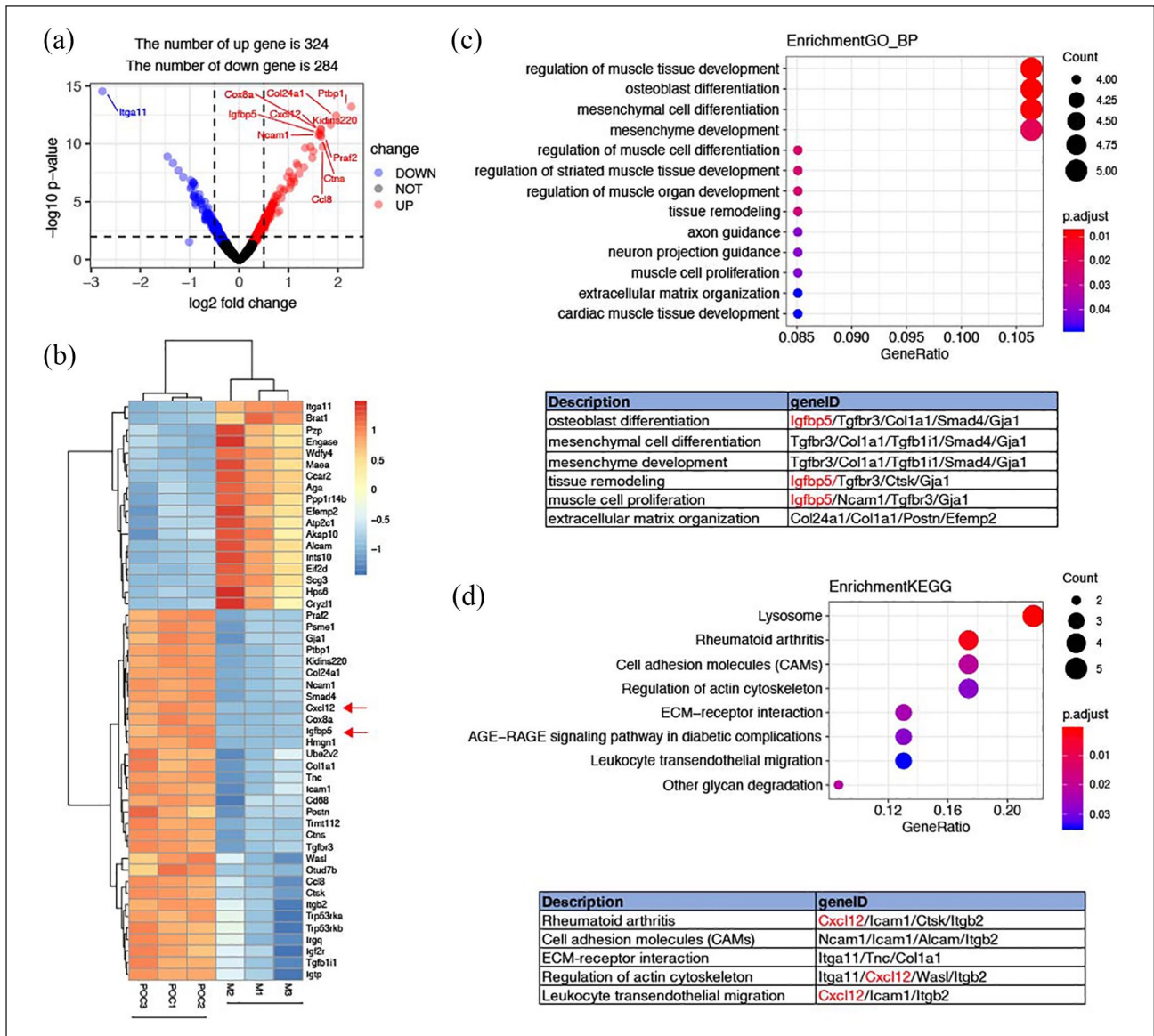


**Figure 4.** Proteomic analysis of ECM-based TEBs. (a) Volcano plot for the differential proteins profile. (b) Heatmap of the top 50 differentially expressed proteins. (c) Gene Ontology (GO) enrichment of the 608 differentially expressed proteins. (d) KEGG enrichment of the 608 differentially expressed proteins.

However, a more rapid release in MSC ECM-based TEBs and a cumulative total protein reached a peak on the third day. As for CXCL12, the release durations were approximately 12 days, while the introduction of POCs delivered more CXCL12 (Figure 5(a)). Co-cultivation results revealed POCs secreted more IGFBP5 and CXCL12, owing to the indirect interaction with BMMSCs. At the same time, BMMSCs were not sensitive to this interaction (Figure 5(b)).

Furthermore, in order to verify the effect of IGFBP5 on osteoblastic differentiation of BMMSCs, neutralizing antibodies were used to block its vitality. A decrease in the expression of the osteogenic differentiation-expressing gene was obtained on the addition of the antibody, which

was in line with the results of the Alizarin Red S staining and the calcium-cobalt ALP staining (Figure 5(c) and (d)). CXCL12 promoted BMMSCs migration and the findings were confirmed in wound healing assay and transwell migration assay results (Figure 5(e) and (f)).

## Discussion

MSC-based TEBs, as a research hotspot, suffered from several limitations.<sup>20–22</sup> The observation of massive cell death during storage and transportation prompted us to adopt alternative methods. Increasing evidence showed that ECM-based TEB was capable of delivering biological signals, such as cell adhesion sites, which is analogous to

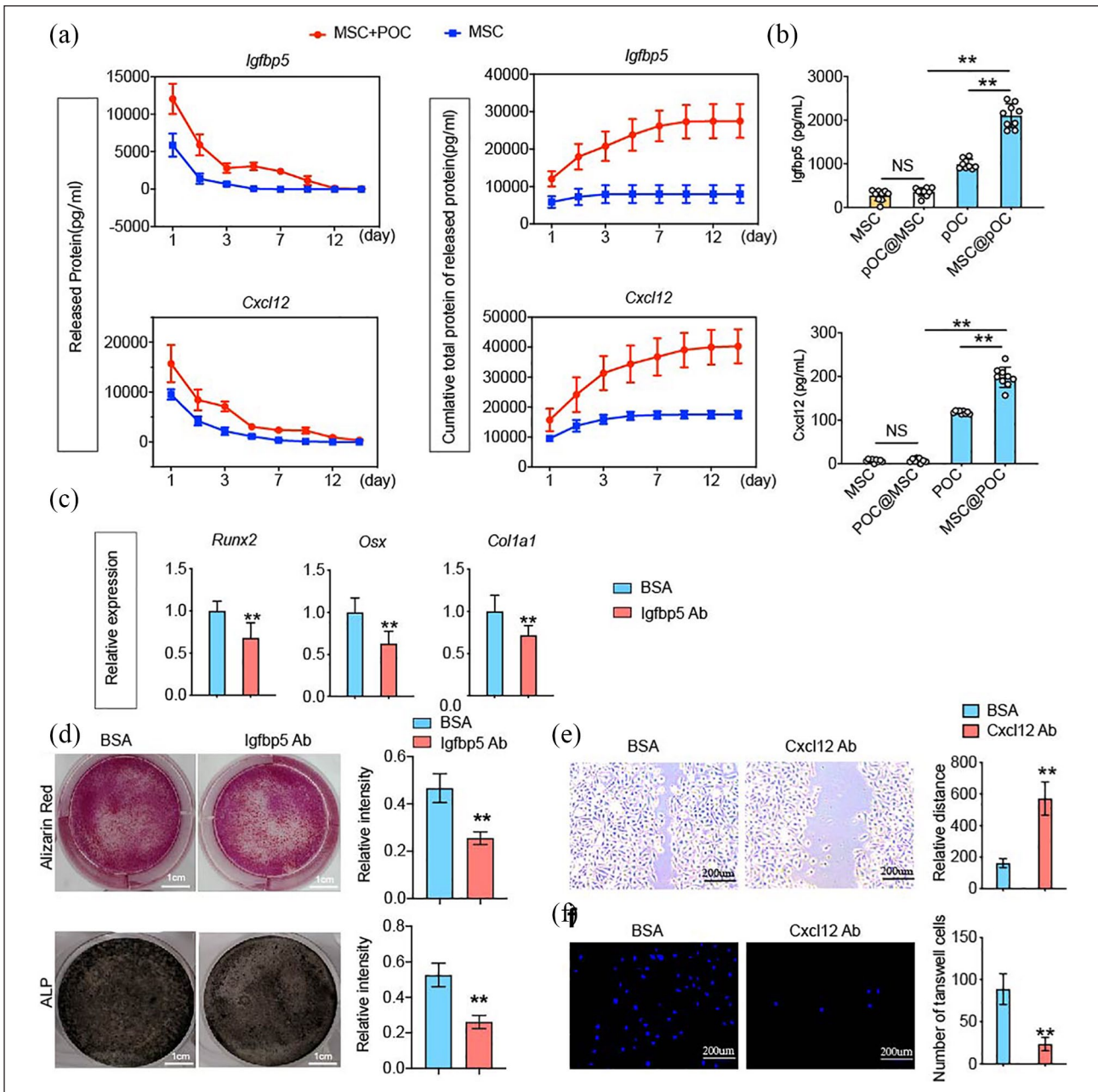


**Figure 5.** IGFBP5 and CXCL12 released from the MSC/POC ECM-based TEBS enhanced the osteogenic differentiation and migration. (a) Release profiles and cumulative total proteins of IGFBP5 and CXCL12 over 15 days. (b) POCs released more IGFBP5 and CXCL12 owing to the indirect co-culture with MSCs. (c) IGFBP5 antibody reduced the expression of osteogenic marker genes, including Runx2, Col1a1, and Osx, GAPDH was used as a loading control. (d) Representative images and qualitative analysis of MSC Alizarin Red S staining and ALP staining. Scale bars are 1 cm. (e, f) Qualitative analysis of the MSC invasion ability by the transwell assay and the migration ability by the wound healing assay. Scale bars are 200  $\mu$ m. \*\* $p < 0.01$ , \* $p < 0.05$ , NS: no significance.

bone regeneration microenvironments and a new strategy for tissue repair.<sup>23–26</sup> Previous studies conducted by our group have found that MSC ECM-based TEBS released a variety of active proteins with osteogenesis activity and increased osteoinductivity. In the present study, we demonstrated that MSC/POC ECM-based TEBS significantly enhanced osteogenesis in a rat femur defect model compared with MSC ECM-based TEBS. Moreover, it has been

reported that Runx2 began to decline on day 16 during osteogenic differentiation, similar to OSX. However, Col1a1 decreased only at the terminal differentiation stage. We chose the 14-day time point for testing osteogenic marker genes and staining to try to reflect both the degree of osteogenic differentiation and the accumulation of type I collagen *in vitro* experiments.<sup>27</sup> Furthermore, *in vitro* studies highlighted the fact that active proteins released

from the MSC/POC ECM-based TEBs, especially, IGFBP5 and CXCL12, significantly promoted migration and osteogenic differentiation of BMMSCs.

Moreover, repairing critical-size segmental bone defects requires enormous amounts of MSCs, which compels us to face the problem of limited sources in seed cells.<sup>28,29</sup> On the one hand, insufficient oxygen and blood flow in the microenvironment within the defected bone contributed to the death of a high percentage of MSCs, ultimately leading to the failure of treatment. On the other hand, a limitation also exists in storage and transportation due to the viability of MSCs.<sup>30</sup> Therefore, we employed lyophilization to reduce the antigenicity of cell-based scaffolds. After lyophilization, the significant antigens (MHC-I and MHC-II) causing an immune rejection reduced. DAPI staining also revealed that another important antigenic substance (DNA) was almost exhausted. Then, we analyzed histocompatibility by the MLR method and DNA quantification assay, and these results added credence to the view that decellularization significantly enhanced the histocompatibility.

Recently, OCs have been recognized as essential participants in bone remodelling and repair.<sup>31</sup> Evidence also suggests that preosteoclasts can trigger blood vessels and nerves to promote bone formation.<sup>32</sup> No one has so far applied MSCs and POCs together as seed cells for tissue-engineered bone. Considering the functional role of preosteoclasts in bone homeostasis and bone repair, we introduced osteoclast precursors in combination with MSCs to develop MSC/POC ECM-based TEBs to enhance osteogenesis. Micro-CT 3D reconstruction and histological examinations of this study verified that the application of MSC/POC ECM-based TEBs significantly enhanced bone regeneration when compared with MSC ECM-based TEBs *in vivo*.

We further investigated to elucidate the molecular mechanism behind the enhancement of osteogenesis by MSC/POC ECM-based TEBs. Bioinformatics analysis manifested that these distinctly different proteins between MSC/POC ECM-based TEBs and MSC ECM-based TEBs are primarily associated with osteogenic differentiation, cell migration, cell adhesion, and ECM-receptor interactions. IGFBP5 and CXCL12 appeared most frequently among all enriched signaling pathways. Evidence suggests that IGFBP5 also stimulates osteoblasts activity and bone proliferation in ovariectomized mice.<sup>33</sup> Based on *in vitro* and *in vivo* studies, most of IGFBP5 was found to be secreted by preosteoclasts. These proteins get accumulated in the bone matrix and indeed promote BMMSCs osteogenic differentiation, which indicate IGFBP5 may be necessary for healthy bone remodeling.<sup>34-36</sup> Therefore, we hypothesize that IGFBP5 plays a leading role in the intensive osteogenic effect of the MSC/POC combination. On the one hand, the effect of this proteins on the osteogenic differentiation was then investigated by neutralizing antibodies and it was observed that the osteogenic genes

expressions of BMMSCs, including Runx2, Osx, and Col1a1, were partially inhibited, which was in agreement with Alizarin Red S staining and ALP staining results. On the other hand, IGFBP5 antibody may inhibit cell proliferation and facilitate apoptosis of MSCs through activating the ERK/MAPK axis, which could be partly responsible for the decreased in ALP and Alizarin Red S staining.<sup>37,38</sup> At the same time, we can also conclude that MSC/POC ECM-based TEBs enhanced osteogenesis cannot be attributed entirely to IGFBP5 and there are other mechanisms, yet to be explored.

ECM-based TEBs are more likely to recruit host cells to participate in tissue repair compared to cell-based tissue engineering therapy.<sup>39</sup> Abundant evidence has suggested that the CXCL12-CXCR4 axis is an essential regulator of cell mobilization and chemotaxis during tissue regeneration, which makes widespread use of CXCL12 in engineering regenerative medicine technologies.<sup>40,41</sup> In the present study, CXCL12 was significantly elevated in the MSC/POC group and played a crucial role in recruiting host cells for bone regeneration, as detected through the ELISA kit and neutralizing antibody. *In vitro* experiments showed that the migration of BMMSCs was visibly inhibited after the addition of a neutralization antibody for CXCL12. All these findings indicated that CXCL12 is a vital recruitment factor.

It is well-known that cell adhesion is critical for tissue-engineered bone. The surface characteristics of the scaffolds determine cell shape and proliferation to maintain proper cellular function and tissue integrity.<sup>42,43</sup> Without strong stickiness, a series of cellular events may not occur in a dynamic environment. CAMs anchor cells to the matrix and send location signals that direct cell transportation and differentiation.<sup>44</sup> Our study showed a significant upregulation of cell adhesion molecules in MSC/POC ECM-based TEBs, including NCAM1, ICAM1, ALCAM, and ITGB2, which were in line with cell adhesion results observed *in vitro*. Further in-depth research is needed to confirm the role of CAMs on ECM-based TEBs for participating in bone repair.

## Conclusion

In this present study, we provided evidence that MSC/POC ECM-based TEBs visibly promoted bone regeneration in a rat model of femoral defects. The underlying mechanism appeared to be the activation and recruitment of endogenous BMMSCs at the bone defect site, which was also verified by the biological function of soluble proteins released from ECM-based TEBs. Furthermore, CXCL12 and IGFBP5 from MSC/POC ECM-based TEBs participated in the recruitment of host cells and promoted osteogenic differentiation during bone regeneration, respectively. We optimize the ECM-based TEBs by introducing POCs, which will provide new insight for bone tissue engineering.

## Declaration of conflicting interests

The author(s) declared no potential conflicts of interest with respect to the research, authorship, and/or publication of this article.

## Funding

The author(s) disclosed receipt of the following financial support for the research, authorship, and/or publication of this article: This work was funded by the State Key Program of National Natural Science of China (No. 81930067), the National Natural Science Foundation of China (No. 31870962), the Key Project of Logistics Research Plan of the PLA (No. AWS17J004), the Innovation Funding of TMMU (No. 2018XYY05), the Medical Science and Technology Youth Cultivation Project of PLA (No. 20QNPY022) and Medical Innovation Capability Upgrading Plan of Southwest Hospital (No. SWH2018LJ-03).

## ORCID iD

Shiwu Dong  <https://orcid.org/0000-0002-5032-4893>

## Supplemental material

Supplemental material for this article is available online.

## References

1. Yang F, Wang J, Hou J, et al. Bone regeneration using cell-mediated responsive degradable PEG-based scaffolds incorporating with rhBMP-2. *Biomaterials* 2013; 34(5): 1514–1528.
2. Bose S and Sarkar N. Natural medicinal compounds in bone tissue engineering. *Trends Biotechnol* 2020; 38: 404–417.
3. Marolt Presen D, Traweger A, Gimona M, et al. Mesenchymal stromal cell-based bone regeneration therapies: from cell transplantation and tissue engineering to therapeutic secretomes and extracellular vesicles. *Front Bioeng Biotechnol* 2019; 7: 352.
4. Cunniffe GM, Diaz-Payno PJ, Sheehy EJ, et al. Tissue-specific extracellular matrix scaffolds for the regeneration of spatially complex musculoskeletal tissues. *Biomaterials* 2019; 188: 63–73.
5. Shakouri-Motlagh A, O'Connor AJ, Brennecke SP, et al. Native and solubilized decellularized extracellular matrix: a critical assessment of their potential for improving the expansion of mesenchymal stem cells. *Acta Biomater* 2017; 55: 1–12.
6. Vainieri ML, Lolli A, Kops N, et al. Evaluation of biomimetic hyaluronic-based hydrogels with enhanced endogenous cell recruitment and cartilage matrix formation. *Acta Biomater* 2020; 101: 293–303.
7. Zhang X, Wang C, Liao M, et al. Aligned electrospun cellulose scaffolds coated with rhBMP-2 for both in vitro and in vivo bone tissue engineering. *Carbohydr Polym* 2019; 213: 27–38.
8. Sims NA and Martin TJ. Osteoclasts provide coupling signals to osteoblast lineage cells through multiple mechanisms. *Annu Rev Physiol* 2020; 82: 507–529.
9. Lymperi S, Ersek A, Ferraro F, et al. Inhibition of osteoclast function reduces hematopoietic stem cell numbers in vivo. *Blood* 2011; 117(5): 1540–1549.
10. Bozec A, Zaiss MM, Kagwiria R, et al. T cell costimulation molecules CD80/86 inhibit osteoclast differentiation by inducing the IDO/tryptophan pathway. *Sci Transl Med* 2014; 6(235): 235–260.
11. Schneider JG, Amend SR and Weilbaecher KN. Integrins and bone metastasis: integrating tumor cell and stromal cell interactions. *Bone* 2011; 48(1): 54–65.
12. Xie H, Cui Z, Wang L, et al. PDGF-BB secreted by pre-osteoclasts induces angiogenesis during coupling with osteogenesis. *Nat Med* 2014; 20(11): 1270–1278.
13. Dou C, Ding N, Luo F, et al. Graphene-based microRNA transfection blocks preosteoclast fusion to increase bone formation and vascularization. *Adv Sci (Weinh)* 2018; 5(2): 1700578.
14. Dou C, Ding N, Zhao C, et al. estrogen deficiency-mediated M2 macrophage osteoclastogenesis contributes to M1/M2 ratio alteration in ovariectomized osteoporotic mice. *J Bone Miner Res* 2018; 33(5): 899–908.
15. Huang J, Yin H, Rao SS, et al. Harmine enhances type H vessel formation and prevents bone loss in ovariectomized mice. *Theranostics* 2018; 8(9): 2435–2446.
16. Kang Y, Kim S, Khademhosseini A, et al. Creation of bony microenvironment with CaP and cell-derived ECM to enhance human bone-marrow MSC behavior and delivery of BMP-2. *Biomaterials* 2011; 32(26): 6119–6130.
17. Thaweesapphithak S, Tantrawatpan C, Kheolamai P, et al. Human serum enhances the proliferative capacity and immunomodulatory property of MSCs derived from human placenta and umbilical cord. *Stem Cell Res Ther* 2019; 10(1): 79.
18. Deng M, Chang Z, Hou T, et al. Sustained release of bioactive protein from a lyophilized tissue-engineered construct promotes the osteogenic potential of mesenchymal stem cells. *J Orthop Res* 2016; 34(3): 386–394.
19. Chai YC, Bolander J, Papanтониou I, et al. (\*) Harnessing the osteogenicity of in vitro stem cell-derived mineralized extracellular matrix as 3D biotemplate to guide bone regeneration. *Tissue Eng Part A* 2017; 23(17–18): 874–890.
20. Moradi SL, Golchin A, Hajishafieha Z, et al. Bone tissue engineering: adult stem cells in combination with electrospun nanofibrous scaffolds. *J Cell Physiol* 2018; 233(10): 6509–6522.
21. Wubneh A, Tsekoura EK, Ayranci C, et al. Current state of fabrication technologies and materials for bone tissue engineering. *Acta Biomater* 2018; 80: 1–30.
22. Wang Z, Li Z, Li Z, et al. Cartilaginous extracellular matrix derived from decellularized chondrocyte sheets for the reconstruction of osteochondral defects in rabbits. *Acta Biomater* 2018; 81: 129–145.
23. Kim B, Ventura R and Lee BT. Functionalization of porous BCP scaffold by generating cell-derived extracellular matrix from rat bone marrow stem cells culture for bone tissue engineering. *J Tissue Eng Regen Med* 2018; 12(2): e1256–e1267.
24. Dissanayaka WL, Zhu L, Hargreaves KM, et al. Scaffold-free prevascularized microtissue spheroids for pulp regeneration. *J Dent Res* 2014; 93(12): 1296–1303.
25. Lin X, Zhao C, Zhu P, et al. Periosteum extracellular-matrix-mediated acellular mineralization during bone formation. *Adv Healthc Mater* 2018; 7(4): 1700660.
26. Xu JZ, Qin H, Wang XQ, et al. Repair of large segmental bone defects using bone marrow stromal cells with demineralized bone matrix. *Orthop Surg* 2009; 1(1): 34–41.

27. Maeda T, Matsunuma A, Kurahashi I, et al. Induction of osteoblast differentiation indices by statins in MC3T3-E1 cells. *J Cell Biochem* 2004; 92(3): 458–471.
28. Luo K, Mei T, Li Z, et al. A high-adhesive lysine-cyclic RGD peptide designed for selective cell retention technology. *Tissue Eng Part C Methods* 2016; 22(6): 585–595.
29. Deng M, Mei T, Hou T, et al. TGFbeta3 recruits endogenous mesenchymal stem cells to initiate bone regeneration. *Stem Cell Res Ther* 2017; 8(1): 258.
30. Griffin MD, Ritter T and Mahon BP. Immunological aspects of allogeneic mesenchymal stem cell therapies. *Hum Gene Ther* 2010; 21(12): 1641–1655.
31. Maurizi A and Rucci N. The osteoclast in bone metastasis: player and target. *Cancers (Basel)* 2018; 10(7): 218.
32. Romeo SG, Alawi KM, Rodrigues J, et al. Endothelial proteolytic activity and interaction with non-resorbing osteoclasts mediate bone elongation. *Nat Cell Biol* 2019; 21(4): 430–441.
33. Mohan S, Nakao Y, Honda Y, et al. Studies on the mechanisms by which insulin-like growth factor (IGF) binding protein-4 (IGFBP-4) and IGFBP-5 modulate IGF actions in bone cells. *J Biol Chem* 1995; 270(35): 20424–20431.
34. Richman C, Baylink DJ, Lang K, et al. Recombinant human insulin-like growth factor-binding protein-5 stimulates bone formation parameters in vitro and in vivo. *Endocrinology* 1999; 140(10): 4699–4705.
35. Andress DL and Birnbaum RS. Human osteoblast-derived insulin-like growth factor (IGF) binding protein-5 stimulates osteoblast mitogenesis and potentiates IGF action. *J Biol Chem* 1992; 267(31): 22467–22472.
36. Andress DL. IGF-binding protein-5 stimulates osteoblast activity and bone accretion in ovariectomized mice. *Am J Physiol Endocrinol Metab* 2001; 281(2): E283–E288.
37. Wang T, Wang CJ, Tian S, et al. Overexpressed IGFBP5 promotes cell proliferation and inhibits apoptosis of nucleus pulposus derived from rats with disc degeneration through inactivating the ERK/MAPK axis. *J Cell Biochem* 2019; 120(11): 18782–18792.
38. Han N, Zhang F, Li G, et al. Local application of IGFBP5 protein enhanced periodontal tissue regeneration via increasing the migration, cell proliferation and osteo/dentinogenic differentiation of mesenchymal stem cells in an inflammatory niche. *Stem Cell Res Ther* 2017; 8(1): 210.
39. Kang H, Zeng Y and Varghese S. Functionally graded multilayer scaffolds for in vivo osteochondral tissue engineering. *Acta Biomater* 2018; 78: 365–377.
40. Wegman F, Poldervaart MT, van der Helm YJ, et al. Combination of bone morphogenetic protein-2 plasmid DNA with chemokine CXCL12 creates an additive effect on bone formation onset and volume. *Eur Cell Mater* 2015; 30: 1–10; discussion 10–11.
41. Vashisth P and Bellare JR. Development of hybrid scaffold with biomimetic 3D architecture for bone regeneration. *Nanomedicine* 2018; 14(4): 1325–1336.
42. Bettahalli NM, Arkesteijn IT, Wessling M, et al. Corrugated round fibers to improve cell adhesion and proliferation in tissue engineering scaffolds. *Acta Biomater* 2013; 9(6): 6928–6935.
43. Ruoslahti E and Pierschbacher MD. New perspectives in cell adhesion: RGD and integrins. *Science* 1987; 238(4826): 491–497.
44. Schakenraad JM, Busscher HJ, Wildevuur CR, et al. The influence of substratum surface free energy on growth and spreading of human fibroblasts in the presence and absence of serum proteins. *J Biomed Mater Res* 1986; 20(6): 773–784.